

Theory-agnostic searches for non-gravitational modes in black hole ringdown

Francesco Crescimbeni,^{1,2,*} Xisco Jimenez Forteza,^{3,†} Swetha Bhagwat,^{4,‡} Julian Westerweck,^{4,5,6,§} and Paolo Pani^{1,2,¶}

¹*Dipartimento di Fisica, Sapienza Università di Roma, Piazzale Aldo Moro 5, 00185, Roma, Italy*

²*INFN, Sezione di Roma, Piazzale Aldo Moro 2, 00185, Roma, Italy*

³*Departament de Física, Universitat de les Illes Balears, IAC3 – IEEC, Crta. Valldemossa km 7.5, E-07122 Palma, Spain*

⁴*School of Physics and Astronomy & Institute for Gravitational Wave Astronomy, University of Birmingham, Birmingham, B15 2TT, United Kingdom*

⁵*Max-Planck-Institut für Gravitationsphysik (Albert-Einstein-Institut), Callinstraße 38, D-30167 Hannover, Germany*

⁶*Leibniz Universität Hannover, D-30167 Hannover, Germany*

In any extension of General Relativity (GR), extra fundamental degrees of freedom couple to gravity. Besides deforming GR forecasts in a theory-dependent way, this coupling generically introduces extra modes in the gravitational-wave signal. We propose a novel theory-agnostic test of gravity to search for these nongravitational modes in black hole merger ringdown signals. To leading order in the GR deviations, their frequencies and damping times match those of a test scalar or vector field in a Kerr background, with only amplitudes and phases as free parameters. This test will be highly valuable for future detectors, which will achieve signal-to-noise ratios higher than 100 (and as high as 1000 for space-based detectors such as LISA). Such sensitivity will allow measurement of these modes with amplitude ratios as low as 0.05 for ground-based detectors (and as low as 0.008 for LISA), relative to the fundamental mode, enabling stringent agnostic constraints or detection of scalar/vector modes. By applying this test to GW150914, GW190521, and GW200129, we find that the current evidence for an extra mode is comparable to that for the first gravitational overtone, but its inclusion modifies the inferred remnant spin.

Introduction. The black hole (BH) spectroscopy program [1–4] plays a prominent role in the landscape of strong-field tests of General Relativity (GR) [5–8] and provides a unique method for examining the nature of compact remnants formed post-coalescence [9]. This program focuses on extracting the remnant quasinormal modes (QNMs) [10–13] during the ringdown phase of a binary merger. In the context of linear perturbation theory, the signal $h(t)$ at intermediate times after the merger is represented by a superposition of the QNMs of the remnant [14], as it transitions towards a stationary configuration. Schematically,

$$h(t) = \sum_i A_i \cos(2\pi f_i t + \phi_i) e^{-\frac{t}{\tau_i}}, \quad (1)$$

where A_i , ϕ_i , f_i , τ_i are the amplitude, phase, frequency, and damping time of the i -th QNM. If the remnant is a BH, GR predicts that the infinite spectrum of QNMs is uniquely determined by its mass and spin (M_f, χ_f). This provides opportunities for conducting multiple null-hypothesis tests of gravity [15, 16] and investigating the nature of the remnant [17–19].

As suggested by Lovelock’s theorem [20, 21], an almost unavoidable ingredient of theories beyond GR is the presence of extra degrees of freedom nonminimally coupled to gravity [6, 22]. Examples are ubiquitous and include scalar fields in scalar-tensor theories

and Horndeski’s gravity [23] (and their vector counterpart [24]), high-curvature corrections to GR that predict extra (pseudo)scalars and dilaton fields [25–27], Einstein-Aether [28] and Hořava–Lifshitz [29] gravity that postulate an extra timelike vector field, and massive gravity [30, 31] with both scalar and vector dynamical degrees of freedom (see [6] for a review of GR extensions and their field content). Effective extra degrees of freedom are also unavoidable in any approach that treats GR as the leading order term in an effective-field-theory expansion (e.g., [27]) and in low-energy effective string theories. These nonminimally coupled fields may modify the stationary BH solutions, leading to deviations from the Kerr metric, and/or modify the dynamics of the theory. In either case, two generic predictions are: i) a deformation of the Kerr QNMs,

$$f_i = f_i^{\text{Kerr}}(1 + \delta f_i), \quad \tau_i = \tau_i^{\text{Kerr}}(1 + \delta \tau_i), \quad (2)$$

and ii) the existence of extra modes in the gravitational signal, that can be excited during the ringdown. This second option is due to the fact that the nonminimal coupling between new degrees of freedom and gravity results in coupled systems of linear perturbation equations, which act as a coupled set of oscillators [32–34]. It is therefore natural to split the ringdown signal (1) into two contributions,

$$h(t) = \sum_i A_i \cos(2\pi f_i^{\text{Kerr}}(1 + \delta f_i)t + \phi_i) e^{-\frac{t}{\tau_i^{\text{Kerr}}(1 + \delta \tau_i)}} + \sum_i \hat{A}_i \cos(2\pi \hat{f}_i t + \hat{\phi}_i) e^{-t/\hat{\tau}_i}, \quad (3)$$

where we use the hat to denote quantities related to the extra modes.

* francesco.crescimbeni@uniroma1.it

† f.jimenez@uib.es

‡ s.bhagwat@bham.ac.uk

§ j.m.westerweck@bham.ac.uk

¶ paolo.pani@uniroma1.it

Standard tests of gravity based on the ringdown are rooted in the first line of Eq. (3). Namely, they are aimed at measuring δf_i and $\delta \tau_i$ and check whether they are compatible with the null hypothesis [5]. This can be accomplished in two complementary ways, either through a theory-agnostic or theory-dependent method. However, both approaches have their own limitations. In the theory-agnostic approach one uses the parametrization (2), where f_i^{Kerr} and τ_i^{Kerr} are known functions of the BH mass and spin, while δf_i and $\delta \tau_i$ depend on the mass, spin, and all extra fundamental coupling constants of the theory. It is convenient (and natural, from an effective-field-theory perspective) to restrict to small GR deviations that continuously deform the Kerr result, in which case $\delta f_i, \delta \tau_i \ll 1$ and are proportional to some combination of the mass and coupling constants. However, even in this case they are still generic functions of the spin χ_f . Current parametrizations either neglect such spin dependence [5, 35, 36] or consider a small spin expansion of each deviation [37–39], which inevitably inflates the number of free parameters in the model. In the theory-dependent approach, the QNMs are computed in a given theory of gravity. For most theories this can be done again only in the small-coupling limit and very often perturbatively in the spin [32, 40–49]. To reach good convergence, one needs to push the spin expansion to very high order [48], which is very challenging from the technical point of view. Alternatively, one needs to solve intricate systems of coupled partial differential equations [50–55]. This approach has the benefit of limiting the number of free parameters to the sole coupling constants and BH spin, but must be performed on a case-by-case basis for every given theory.

Given the above limitations, it would be highly desirable to develop complementary ringdown tests which are both theory-agnostic and accurate. In this work we explore a currently unbeaten path, related to the second line of Eq. (3). Namely, we propose to look for extra modes in the ringdown signal, which are not related to deformations of the Kerr ones. For concreteness, let us consider the case of an extra scalar degree of freedom nonminimally coupled to gravity (the same argument applies to other types of fields). Due to the coupling, the gravitational perturbations will contain also scalar modes (e.g., [32, 34, 41, 56] for two concrete examples in theories with quadratic curvature terms),

$$\hat{f}_i = f_i^{\text{Kerr}, s=0}(1 + \delta \hat{f}_i), \quad \hat{\tau}_i = \tau_i^{\text{Kerr}, s=0}(1 + \delta \hat{\tau}_i), \quad (4)$$

where $f_i^{\text{Kerr}, s=0}$ and $\tau_i^{\text{Kerr}, s=0}$ are the QNMs of a test scalar field in the Kerr metric, and also in this case $\delta \hat{f}_i$ and $\delta \hat{\tau}_i$ are complicated, theory-dependent, functions of the mass, spin, and coupling constants. Crucially, in this case the amplitudes \hat{A}_i of these modes are *proportional* to (powers of) the coupling constants [32, 34, 41, 56], and they must vanish in the GR limit. Therefore, to leading order in the corrections, we can neglect $\delta \hat{f}_i$ and $\delta \hat{\tau}_i$, so that the GR deviations are generically parametrized

only by the amplitude of the *test-field* modes. This is precisely what happens in so-called dynamical Chern-Simons gravity [26, 32, 34] (see also Appendix), although it is a generic feature.

The above considerations suggest a novel ringdown test of gravity based on the following waveform model

$$h(t) = \sum_i A_i \cos(2\pi f_i^{\text{Kerr}} t + \phi_i) e^{-\frac{t}{\tau_i^{\text{Kerr}}}} + \sum_i \hat{A}_i \cos(2\pi f_i^{\text{Kerr}, s=0} t + \hat{\phi}_i) e^{-\frac{t}{\tau_i^{\text{Kerr}, s=0}}} \quad (5)$$

where for simplicity we have neglected the GR deviations in the first line, since those are very well studied by standard ringdown tests (and subjected to the aforementioned limitations). In practice, here we will focus on a standard GR ringdown waveform (first line of Eq. (5)) augmented by new extra modes. Remarkably, to leading order these extra modes are *known* functions of the BH mass and spin, since they are those of a free test (scalar, vector, etc) field propagating on the Kerr metric (see, e.g., [57, 58] for tabulated values). This allows searching for extra modes in a theory-agnostic way, where the amplitudes and phases of the extra modes are the only beyond-GR parameters. In this sense, this test is reminiscent of searches for extra (scalar, vector) polarizations in GW signals in a theory-agnostic fashion [5, 59–61] and is complementary to ordinary ringdown tests (see, e.g., [5, 35, 36, 62–65]), or to test with multiple free modes [5].

Searching for extra ringdown modes. The ringdown signal comprises of two polarizations and the modes are decomposed in a basis of spin-weighted spheroidal harmonics that depend on the remnant spin inclination angle [65]. Each mode is identified by three integers, $i \equiv (lmn)$, namely the multipolar, azimuthal, and overtone index, respectively, where $n = 0$ corresponds to the fundamental tone and $(lmn) = (220)$ is the dominant mode in a non-precessing quasicircular coalescence. For concreteness, here we focus on the most interesting quadrupolar ($l = 2$) case and neglect spin precession of the progenitor binary, but our test can be applied also to higher-order modes and to the precessing case (see Appendix). In particular, our ringdown waveform model has the following parameters:

$$\underline{\theta} = \{M_f, \chi_f, A_{22j}, \phi_{22j}, \hat{A}_{220}^{s=0,1}, \hat{\phi}_{220}^{s=0,1}\} \quad (6)$$

where $j = 0, \dots, N$, with N the total number of overtones, whereas $\hat{A}_{220}^{s=0,1}$ and $\hat{\phi}_{220}^{s=0,1}$ are the amplitude and phase of the extra scalar ($s = 0$) or vector ($s = 1$) (220) mode. We will dub a model with N tones and no extra mode GRN, whereas we will denote as GRN+S (GRN+V) a model with N gravitational tones and an extra scalar (vector) mode. In practice, we define the amplitude ratio A_R of a given mode relative to the gravitational fundamental one. We fix the luminosity distance d_L , the sky location of the system, and the inclination angle. Note

that, for small-redshift sources (including those detected so far and presumably the loudest events detected in the future) d_L is degenerate with the overall ringdown amplitude and can therefore be neglected without loss of generality. However, the possibility of neglecting inclination angle is a prerogative of our test, since it involves only ($l = m = 2$) modes, which have the same pattern functions and spheroidal-harmonic decomposition. Compared to common tests based on subleading modes of different (l, m), this allows for the practical simplification of sampling in only one of these three degenerate parameters.

The frequencies and damping times of the relevant modes are shown in the Appendix. At variance with overtones, the frequency of the (220) scalar or vector mode is always well separated from that of the fundamental gravitational mode (and hence more easily resolvable from the latter), while the damping time is comparable (and hence the mode survives longer than overtones in the signal, almost as long as the fundamental gravitational mode).

Bayesian analysis on real data. We exemplify our test on real events by performing a Bayesian parameter estimation using the `PyCBC Inference` code infrastructure [66]. The analysis aims to compute the posterior distribution of the parameters (6). We apply this test to three events: (i) GW150914 [67], the first GW event ever detected by LIGO (and still so far the one with the largest ringdown signal-to-noise ratio (SNR)), for which some debated evidence of overtones has been reported [15, 35, 65, 68–76]; (ii) GW190521 [77], a peculiar event in the upper mass gap for which a tentative detection of the (330) and other modes (and possibly precession) has been obtained [78, 79] and which is prone also to ringdown amplitude-phase consistency tests [64]; (iii) GW200129, a peculiar loud event showing some tension with GR in some inspiral-merger-ringdown tests [5], tentatively ascribed to mismodelling of precession [80, 81]. As a proof of principle for the test, our parametrization assumes plane reflection symmetry, which is valid for spin-aligned progenitor binaries. In the Appendix we show that relaxing this assumption does not affect the results for GW190521 and GW200129. For the luminosity distance, inclination, and sky location we adopt the maximum likelihood values reported in [82].

We use a gated-and-inpainted Gaussian likelihood noise model [78, 83, 84] to remove the influence of the pre-peak/non-ringdown times. The strain data within a time interval $t \in [t_c + t_{\text{offset}} - 0.5s, t_c + t_{\text{offset}}]$ are replaced/inpainted such that the filtered inverse power spectral density is zero at all the times corresponding to the chosen interval [84]. Here, t_c is the coalescence time, while t_{offset} defines the time in which we start our ringdown analysis.

Our main results are summarized in Fig. 1, presenting the statistical evidence for different waveform models for these events and for different choices of t_{offset} . We show $\log_{10} \mathcal{B}_{\text{GR1}}^{\text{Model}}$, where the Bayes factor $\mathcal{B}_{\text{GR1}}^{\text{Model}}$ is the ratio between the evidence of a given model and that

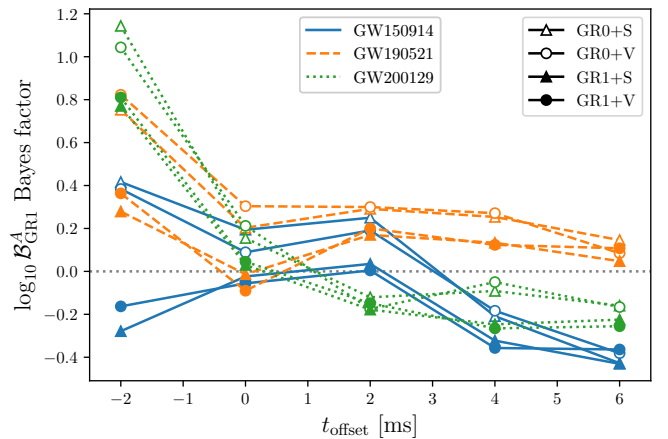


FIG. 1. \log_{10} Bayes factors for various ringdown models with extra scalar or vector modes with respect to the GR1 model as a function of the offset time t_{offset} . Different colors and line styles denote different events, while different markers show the chosen model.

of GR1 (i.e., a model containing only the fundamental gravitational mode and the first overtone). According to Jeffreys’ scale criterion [86], a \log_{10} Bayes factor larger than 1 (resp., 2) would imply a strong (resp., decisive) Bayesian evidence in favor of a given model relative to GR1. The small values of $\log_{10} \mathcal{B}_{\text{GR1}}^{\text{Model}}$ shown in Fig. 1 for any t_{offset} indicate that all models with extra scalar or vector modes have the same evidence as the GR1 one, presumably because the SNR in the ringdown for these events is not sufficiently high to exclude the presence of an extra scalar mode. This is consistent with what we shall discuss below with synthetic data.

Model	$M_f (M_\odot)$	χ_f	$A_{220} \times 10^{20}$	$A_{R,220}$
GR1	58^{+27}_{-22}	$0.35^{+0.49}_{-1.15}$	$0.72^{+0.98}_{-0.50}$	-
GR0+S	52^{+35}_{-16}	$-0.18^{+0.94}_{-0.69}$	$0.69^{+1.32}_{-0.57}$	$0.80^{+2.74}_{-0.64}$
GR1+S	52^{+33}_{-16}	$-0.11^{+0.84}_{-0.76}$	$0.72^{+1.30}_{-0.60}$	$1.95^{+1.85}_{-1.75}$

TABLE I. 90% credible intervals for some of the parameters of event GW150914, assuming $t_{\text{offset}} = 2$ ms (see Appendix for the posterior distributions). We denote the amplitude ratio of the scalar-to-tensor mode as $A_{R,220} = \hat{A}_{220}^{s=0} / A_{220}$.

Interestingly, despite Fig. 1 showing that there is no statistical evidence for an extra scalar or vector mode, its inclusion affects the posterior distributions of the parameters. This is shown in Table I for a representative example of GW150914 analyzed with an extra scalar mode. Other events, different time offsets, or the vector case show qualitatively similar results. While the presence of an extra mode does not affect the distribution of the remnant mass significantly, it contributes to broaden up that of the spin towards smaller values (see Appendix for the posterior distributions). This generic feature can be understood from the fact that an extra (220) scalar/vector mode has a damping time comparable to the fundamen-

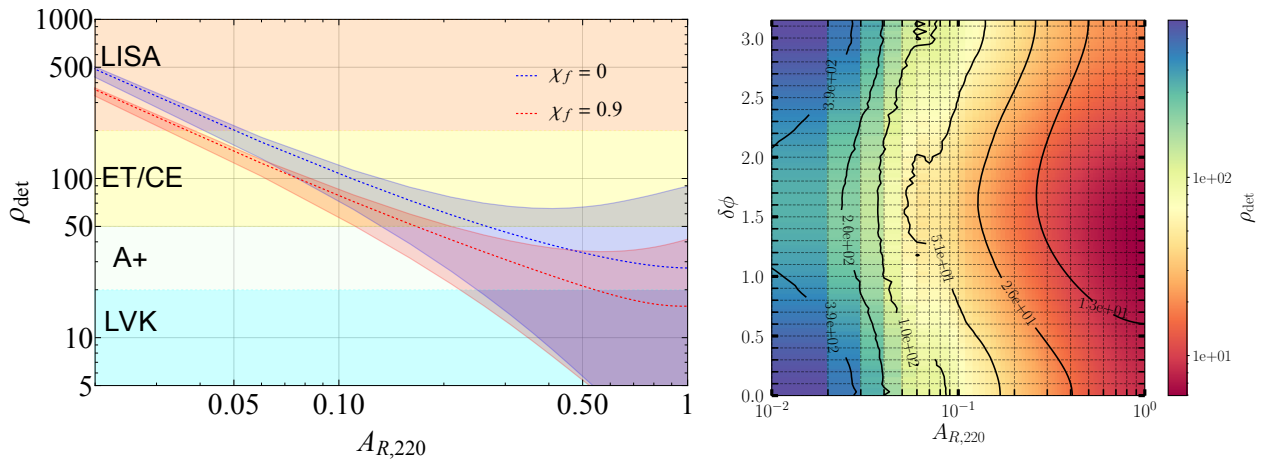


FIG. 2. Left panel: Minimum SNR necessary for detecting a scalar mode at $1-\sigma$ confidence level, according to the detectability criterion outlined in [85] using a Fisher matrix approximation. We take as a reference an event with remnant mass $M_f = 62M_\odot$ for a range of amplitude ratios $A_{R,220} \in [0.02, 1]$. The blue and red dashed curves denote a different remnant spin χ_f with the phase difference between the GR and scalar modes fixed to $\delta\phi = 0$. The dependence on $\delta\phi \in [0, 2\pi]$ is bracketed by the corresponding colored bands. The horizontal shaded bands represent the typical ringdown SNR expected for a GW150914-like event observed by the LVK network at design sensitivity (light blue), A+ (light green), ground-based third-generation observatories as ET/CE (yellow), and for a mass-rescaled version of GW150914 with $10^5 M_\odot$ for LISA (orange). Right: The same quantity shown in a contour plot on the $(A_{R,220}, \delta\phi)$ plane for fixed $\chi_f = 0.67$.

tal gravitational mode (and the damping time is only mildly sensitive to the spin for $\chi_f \lesssim 0.8$) and also has a higher frequency than the (220) and (221) gravitational modes. Thus, interpreting the overtone frequency with an extra scalar/vector mode requires a smaller remnant spin. Also, the amplitude of the fundamental gravitational mode is affected by the extra mode: in the GR0+S and GR1+S models the peak of the A_{220} distribution is smaller because part of the information is contained in the scalar mode. Consequently, the amplitude ratio $A_{R,220}$ between the (220) scalar mode and the (220) gravitational mode peaks at some nonzero value.

Forecasts with future observations. In Fig. 2, we forecast the constraining power of this test by computing the minimum ringdown SNR, ρ_{det} , for detectability of an extra scalar mode in the GR0+S model, for different amplitude ratios, remnant spins, and phase differences $\delta\phi = \phi_{220} - \hat{\phi}_{220}^{s=0}$. (Hereafter we focus on the scalar case, since the vector case gives qualitatively similar results, see Appendix.) ρ_{det} is defined following Refs. [85, 87, 88], namely as the SNR such that $\sigma_{A_R} = A_{R,220}$, where the statistical error σ_{A_R} has been computed with a fully numerical Fisher information matrix [87, 88]. Note that, in contrast to overtones [70, 85], *resolving* the scalar mode is relatively easy since the frequency is significantly different from the gravitational one. For this reason, ρ_{det} is always larger than the SNR threshold required to resolve the extra scalar mode. We perform two variants of this analysis, either averaging over or fixing the sky-location of the signal, with results shown in the left and right panel of Fig. 2, respectively.

The left panel of Fig. 2 shows that ρ_{det} decreases monotonically as χ_f increases – so highly spinning remnants

favor this test – and that the phase difference $\delta\phi$ has a negligible impact for small amplitude ratios, while it can significantly affect the SNR at large amplitudes, especially for slowly-spinning remnants. The dependence on $\delta\phi$ can be better appreciated from the right panel of Fig. 2, showing a contour plot of the two-dimensional function $\rho_{\text{det}}(A_{R,220}, \delta\phi)$ for $\chi_f = 0.67$. In the region of small amplitude ratios, the minimum SNR has a very simple scaling

$$\rho_{\text{det}} \approx 9.3 \frac{g(\chi_f, \delta\phi, A_{R,220})}{A_{R,220}}. \quad (7)$$

where $g \approx 1 + 0.56A_{R,220} - 0.32\chi_f + 0.14 \cos(\delta\phi + 0.98)$, and for $A_{R,220} \leq 0.12$ and $\chi_f \leq 0.9$ the fit is accurate within 10%.

In the left panel of Fig. 2 we also provide reference values of the ringdown SNR for current and future detectors. In particular, third-generation ground-based detectors [89] such as Cosmic Explorer [90–92] and the Einstein Telescope [93–95] are expected to observe a few events per year with ringdown SNR greater than 100 [88]. Likewise, GW space interferometers such as LISA [96] are expected to detect up to a dozen of massive BH mergers with ringdown SNR greater than 1000, depending on the massive BH population [87, 97]. Our results show that a ringdown SNR of 150 (resp., 1000) would yield a constraint $A_{R,220} \lesssim 0.05$ (resp., 0.008) for $\chi_f \approx 0.9$, with only mild dependence on $\delta\phi$. Very similar results apply to the detectability of an extra vector mode.

This plot also confirms that the constraining power of the test is very limited when the ringdown SNR is around 10, which is a rough and even optimistic estimate for the

previously analyzed events GW150914, GW190521, and GW200129.

While these results were obtained using a Fisher-matrix approximation to explore the entire parameter space, we have also compared individual points with synthetic injections at zero noise using the same Bayesian analysis discussed above for real-data events. At SNRs of $1.25\rho_{\text{det}}$ as given in Fig. 2, we find posteriors of A_R peaking away from the lower bound and $\sigma_{A_R} \lesssim A_{R,220}$, already in agreement with the expectation from the Fisher analysis for the high-SNR limit.

Discussion. Any theory predicting extra ringdown modes should presumably also predict deviations from the standard gravitational Kerr QNMs, in which case one could argue that GW detectors are more sensitive to phase differences (and hence to QNM shifts) rather than amplitude differences, so that our test could have less constraining power than ordinary ringdown tests. However, there are known examples of theories predicting zero or negligible QNM shifts but extra modes, in which case our test can be superior to ordinary BH spectroscopy. An example is dynamical Chern-Simons gravity, wherein for a Schwarzschild BH the GR QNMs are unchanged, but the ordinary ringdown contains also extra scalar modes [32]. In the Kerr case also the GR QNMs are modified, but the deviations are suppressed by powers of the BH spin [45], so the convenience of our method will likely depend on the remnant’s spin.

As future extensions, it would be interesting to consider a specific theory and compare the constraints on the coupling constant(s) placed by our test with those of ordinary BH spectroscopy. This would require estimates of both ordinary QNM shifts and excitation amplitudes of extra modes in a given theory, both of which have recently become available for some theories [47–49, 98–105]. Another possible avenue of exploration is to use the recently introduced QNM filtering technique [35, 36, 76] to search for extra (scalar, vector, etc) modes.

Acknowledgements. We thank Collin Capano and Alexander Nitz for clarifications on PyCBC inference, and Gregorio Carullo, Cecilia Chirenti, Gabriele Franciolini, Nico Yunes, and the participants of the workshop [Ringdown Inside and Out](#) for insightful comments and discussions. This work is partially supported by the MUR PRIN Grant 2020KR4KN2 “String Theory as a bridge between Gauge Theories and Quantum Gravity”, by the FARE programme (GW-NEXT, CUP: B84I20000100001), and by the INFN TEON-GRV initiative. X. Jimenez is supported by the Spanish Ministerio de Ciencia, Innovación y Universidades (Beatriz Galindo, BG22-00034) and cofinanced by UIB; the Spanish Agencia Estatal de Investigación Grants No. PID2022-138626NB-I00, No. RED2022-134204-E, and No. RED2022-134411-T, funded by MCIN/AEI/10.13039/501100011033/FEDER, UE; the MCIN with funding from the European Union NextGenerationEU/PRTR (No. PRTR-C17.I1); the Comunitat Autònoma de les Illes Balears through the Direcció Gen-

eral de Recerca, Innovació i Transformació Digital with funds from the Tourist Stay Tax Law (No. PDR2020/11 - ITS2017-006), and the Conselleria d’Economia, Hisenda i Innovació Grant No. SINCO2022/6719. Some numerical computations have been performed at the Vera cluster supported by the Italian Ministry of Research and by Sapienza University of Rome, and with the University of Birmingham’s BlueBEAR HPC service.

Appendix A: Supplemental material

1. Explicit example: Dynamical Chern-Simons gravity

We provide here a specific example of a nonminimal coupling giving rise to extra scalar modes in the gravitational sector. We consider a theory with quadratic curvature corrections, dynamical Chern-Simons gravity, described by the action [26]

$$S = \frac{1}{16\pi} \int d^4x \sqrt{-g} R - \frac{1}{2} \int d^4x \sqrt{-g} g^{ab} \nabla_a \vartheta \nabla_b \vartheta + \frac{\alpha}{4} \int d^4x \sqrt{-g} \vartheta {}^*RR. \quad (\text{A1})$$

where ϑ is the scalar field, ${}^*RR = \frac{1}{2} R_{abcd} \epsilon^{baef} R^cd_{ef}$ is an odd-parity quadratic-curvature invariant, and α is the coupling constant, with dimensions of a squared mass (henceforth we adopt $G = c = 1$ units).

As in the GR case, the only stationary, spherically-symmetric solution is the Schwarzschild metric. For simplicity we consider perturbations of this solution, neglecting the spin of the background. Axial perturbations of the metric are coupled to those of the scalar field. Upon a spherical harmonic decomposition and in the frequency domain, they reduce to the following set of coupled ordinary differential equations [32]

$$\frac{d^2}{dr_*^2} \Psi + \left\{ \omega^2 - f \left[\frac{l(l+1)}{r^2} - \frac{6M}{r^3} \right] \right\} \Psi = \frac{96\pi M f}{r^5} \alpha \Theta, \quad (\text{A2})$$

$$\frac{d^2}{dr_*^2} \Theta + \left\{ \omega^2 - f \left[\frac{l(l+1)}{r^2} \left(1 + \frac{576\pi M^2 \alpha^2}{r^6} \right) + \frac{2M}{r^3} \right] \right\} \Theta = f \frac{(l+2)!}{(l-2)!} \frac{6M\alpha}{r^5} \Psi \quad (\text{A3})$$

where $f(r) = 1 - 2M/r$ and $r_* \equiv r + 2M \ln(r/2M - 1)$ is the standard Schwarzschild tortoise coordinate. The variables Ψ and Θ reduce to the standard metric and scalar master functions, respectively, in the decoupling limit, $\alpha \rightarrow 0$. Indeed, when $\alpha = 0$ the two equations decouple and reduce to the standard Regge-Wheeler equation and scalar-perturbation equation of a Schwarzschild BH, respectively. However, when $\alpha \neq 0$ the two perturbations are coupled to each other and the scalar effective potential acquires some corrections.

The coupling α gives rise to two features [32, 34]:

1. The above system of equations contains both gravity-led and scalar-led modes, both displaying $\mathcal{O}(\alpha^2)$ corrections with respect to GR:

$$\omega = \omega^{\text{GR, grav}} \left(1 + \gamma^{\text{grav}} \frac{\alpha^2}{M^4} \right), \quad (\text{A4})$$

$$\hat{\omega} = \omega^{\text{GR, scal}} \left(1 + \gamma^{\text{scal}} \frac{\alpha^2}{M^4} \right), \quad (\text{A5})$$

where $\omega = 2\pi f - i/\tau$ are the complex QNM frequencies, $\omega^{\text{GR, grav}}$ are the standard Schwarzschild QNMs in GR, $\omega^{\text{GR, scal}}$ are the test-scalar QNMs of Schwarzschild, whereas γ^{grav} and γ^{scal} are dimensionless order-unity constants, the value of which depends on the overtone number n .

2. The above system of equations is akin to a coupled harmonic oscillator, so a scalar perturbation would source scalar modes in the gravitational sector, and vice versa. In particular, in this theory the scalar field is at least linear in α [26], in which case the coupled perturbation equations imply that, whether or not scalar perturbations are

present in the merger conditions (for example if the progenitors are endowed with a scalar field [106]), the amplitude of the scalar mode in the gravitational sector would be $\mathcal{O}(\alpha^2)$. In the notation of the main text, this would imply that, at the leading order, $A_{R,220} \propto \alpha^2/M_f^4$, which is the same order of the usual leading-order corrections to the QNMs in this theory [32, 45, 49].

These arguments show that the *gravitational* ringdown in this theory can be schematically modelled as

$$h(t) = \sum_j A_j e^{i(\omega_j t + \phi_j)} + \sum_j \hat{A}_j e^{i(\hat{\omega}_j t + \hat{\phi}_j)}, \quad (\text{A6})$$

where the sum runs over the overtones. The scalar modes $\hat{\omega}_j$ contains $\mathcal{O}(\alpha^2)$ corrections, but \hat{A}_j is at least $\mathcal{O}(\alpha)$ or higher. Therefore, to leading order in α we can approximate $\hat{\omega}_j \approx \omega_j^{\text{GR, scal}}$ in the second term of the above equation, which is the crucial simplification of our test. This is consistent with the finding of Ref. [32], where the gravitational ringdown in the $\alpha \ll M^2$ limit contains both the *unperturbed* gravitational and scalar modes.

While we explicitly showed this for a specific theory, it is in fact a very general properties of extended theories of gravity with nonminimal couplings (see, e.g., [56] for another example).

2. The effect of precession on GW190521 and GW200129

There are well-founded arguments suggesting that GW190521 and GW200129 could originate from precessing binaries [79, 81]. As opposed to aligned-spin systems,

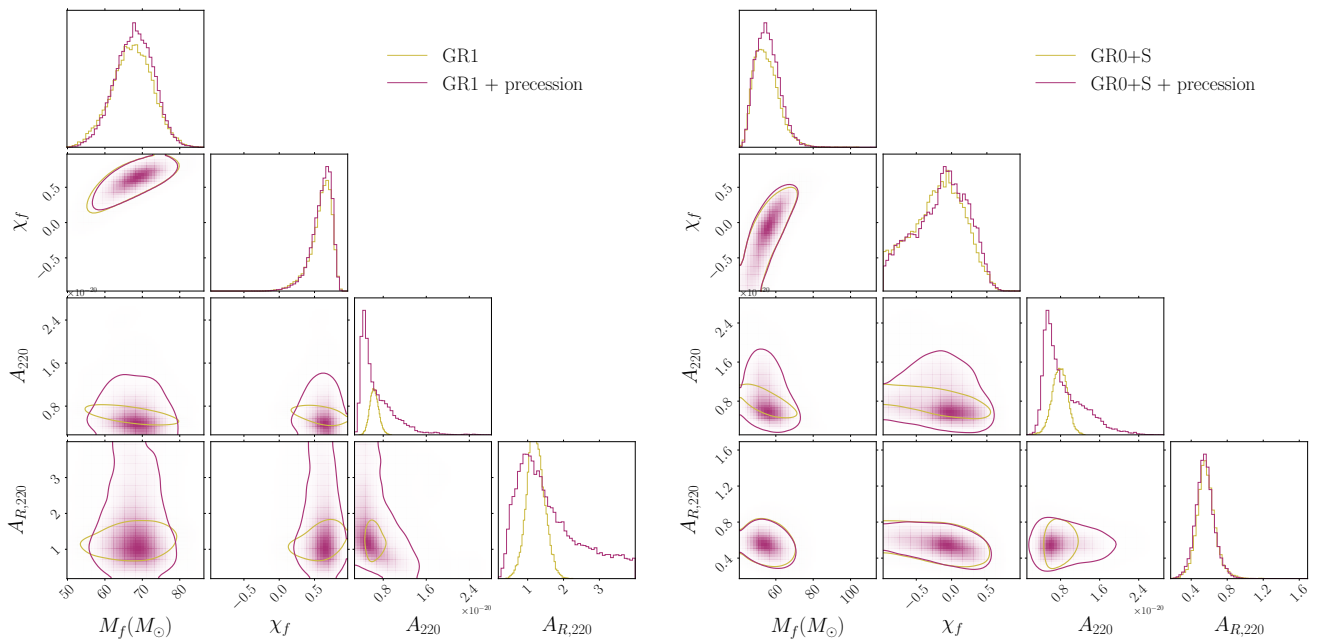


FIG. 3. Posterior distributions for the event GW200129 with $t_{\text{offset}} = 0$ ms for the models GR1 (left) and GR0+S (right). In both cases, the case without (resp., with) precession is indicated in yellow (resp., purple).

precession breaks the symmetry between $m \leftrightarrow -m$ angular modes, resulting in $h_{lm} \neq (-1)^l h_{l-m}^*$. In the main text, we searched for a scalar mode using a $(lm) = (2, \pm 2)$ spin-aligned (non-precessing) waveform. Here, we extend the parameter estimation on GW190521 and GW200129 including precession, and varying $t_{\text{offset}} = [-2, 0, 2]$ ms. This is achieved by allowing the amplitude $A_{22n} \neq A_{2-2n}$ and the phase $\phi_{22n} \neq -\phi_{2-2n}$, for both the gravitational and scalar mode. In Fig. 3, we show the corner plots for GW200129 with $t_{\text{offset}} = 0$, for both the GR01 and GR0+S cases. Notice that, since only $(lm) = (2, \pm 2)$ modes are used, accounting for precession in this case does not significantly affect the values of the mass and the spin of the remnant compared to the aligned-spin case. However, including precession affects the amplitude of the fundamental mode, by increasing its uncertainty. We find qualitatively similar results for the other offset times and for GW190521.

3. Supplemental results

Here we present some results complementing those discussed in the main text.

In Fig. 4 we show the frequencies and damping times of some representative QNMs, including scalar, vector, and gravitational modes as functions of the remnant's

spin. Note that the frequency of the (220) scalar or vector mode is always well separated from that of the fundamental gravitational mode, while its damping time is comparable. These are advantages with respect to overtones, which are instead harder to resolve and decay more rapidly.

Figure 5 presents an example of posterior distributions of some waveform parameters obtained from our Bayesian analysis on real data, namely the case of GW150914 analyzed with various models. Although, as discussed in the main text, there is no statistical evidence for extra scalar modes in the data, their inclusion in the parameter estimation affects the posterior of χ_f and A_{220} .

Finally, in Fig. 6, we compare some representative posterior distributions obtained from the Bayesian inference on real data with forecasts using injections at higher SNR (equal to 100). We consider a ringdown model with an extra scalar mode (GR0+S, left panel) and with an extra vector mode (GR0+V, right panel). For the injection simulations, we inject the values corresponding to the maximum likelihood values of the real data. We notice that, at higher SNRs, the precision of the parameters' distribution improves, and the signal is well reconstructed. This can be easily observed with the distributions of χ_f , which in the case of the real data is spread, due to the effect of the gated Gaussian noise. Also in this case we note that the results for the scalar or vector case are very similar.

[1] O. Dreyer, B. J. Kelly, B. Krishnan, L. S. Finn, D. Garrison, and R. Lopez-Aleman, *Class. Quant. Grav.* **21**,

787 (2004), arXiv:gr-qc/0309007.

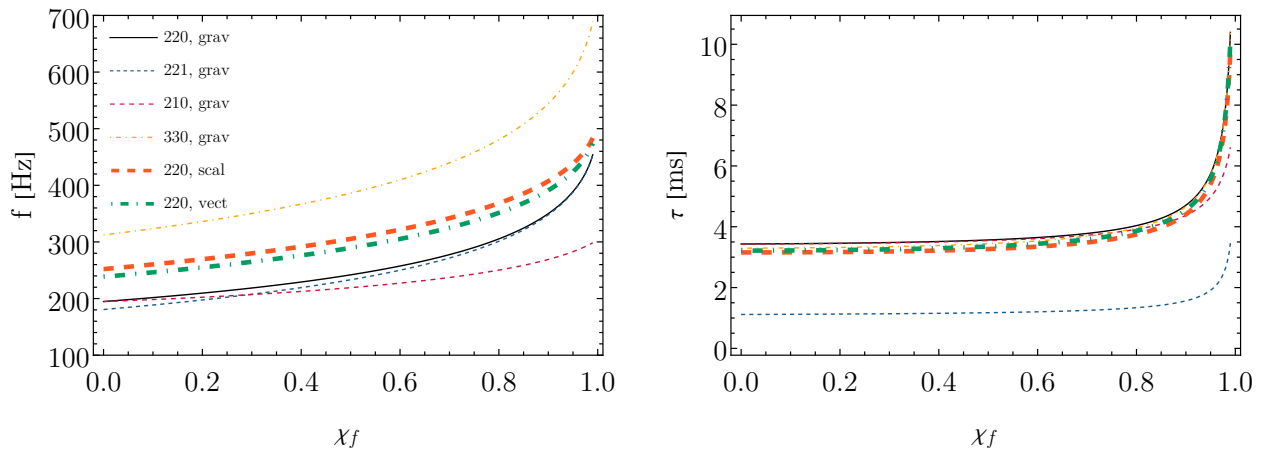


FIG. 4. Frequencies (left) and damping times (right) for a few gravitational modes and for (220) scalar and vector modes of Kerr as a function of the spin. Results are normalized for a remnant mass compatible with GW150914, $M_f = 62 M_\odot$.

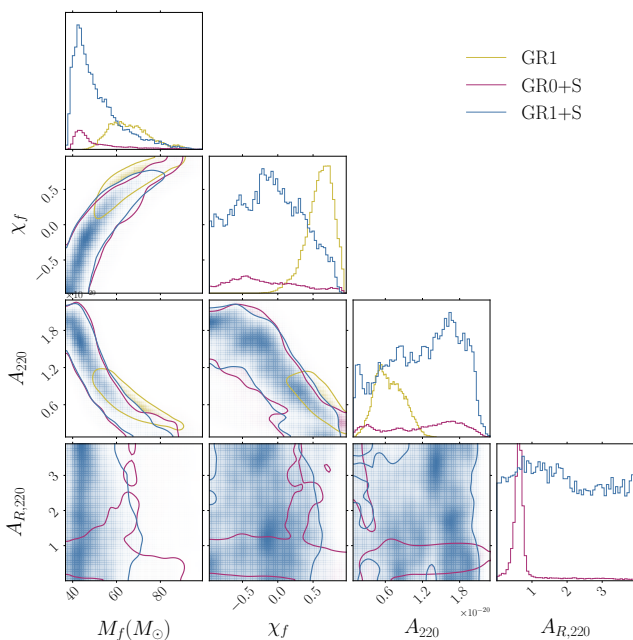


FIG. 5. Posterior distributions of some ringdown parameters for GW150914 in our analysis: M_f and χ_f are the remnant's mass and spin, A_{220} is the amplitude of the fundamental gravitational mode, and A_{220}^R is the amplitude ratio of the (220) scalar mode relative to the fundamental gravitational one. We consider $t_{\text{offset}} = 2$ ms and the GR1 (magenta), GR0+S (yellow), and GR1+S (cyan) models. The contours state the 90% credible levels.

[2] S. L. Detweiler, *Astrophys. J.* **239**, 292 (1980).
 [3] E. Berti, V. Cardoso, and C. M. Will, *Phys. Rev. D* **73**, 064030 (2006), arXiv:gr-qc/0512160.
 [4] S. Gossan, J. Veitch, and B. S. Sathyaprakash, *Phys. Rev. D* **85**, 124056 (2012), arXiv:1111.5819 [gr-qc].
 [5] R. Abbott *et al.* (LIGO Scientific, VIRGO, KAGRA), (2021), arXiv:2112.06861 [gr-qc].

[6] E. Berti *et al.*, *Class. Quant. Grav.* **32**, 243001 (2015), arXiv:1501.07274 [gr-qc].
 [7] E. Berti, K. Yagi, H. Yang, and N. Yunes, *Gen. Rel. Grav.* **50**, 49 (2018), arXiv:1801.03587 [gr-qc].
 [8] M. Colleoni, N. V. Krishnendu, P. Mourier, S. Bera, and X. Jiménez-Forteza, (2024), arXiv:2403.07682 [gr-qc].
 [9] V. Cardoso and P. Pani, *Living Rev. Rel.* **22**, 4 (2019), arXiv:1904.05363 [gr-qc].
 [10] C. V. Vishveshwara, *Nature* **227**, 936 (1970).
 [11] K. D. Kokkotas and B. G. Schmidt, *Living Rev. Rel.* **2**, 2 (1999), arXiv:gr-qc/9909058.
 [12] E. Berti, V. Cardoso, and A. O. Starinets, *Class. Quant. Grav.* **26**, 163001 (2009), arXiv:0905.2975 [gr-qc].
 [13] R. Konoplya and A. Zhidenko, *Rev. Mod. Phys.* **83**, 793 (2011), arXiv:1102.4014 [gr-qc].
 [14] E. W. Leaver, *Phys. Rev. D* **34**, 384 (1986).
 [15] M. Isi, M. Giesler, W. M. Farr, M. A. Scheel, and S. A. Teukolsky, *Phys. Rev. Lett.* **123**, 111102 (2019), arXiv:1905.00869 [gr-qc].
 [16] N. Franchini and S. H. Völkel, (2023), arXiv:2305.01696 [gr-qc].
 [17] E. Maggio, L. Buoninfante, A. Mazumdar, and P. Pani, *Phys. Rev. D* **102**, 064053 (2020), arXiv:2006.14628 [gr-qc].
 [18] E. Maggio, P. Pani, and G. Raposo, (2021), arXiv:2105.06410 [gr-qc].
 [19] E. Maggio, *Lect. Notes Phys.* **1017**, 333 (2023), arXiv:2310.07368 [gr-qc].
 [20] D. Lovelock, *J. Math. Phys.* **12**, 498 (1971).
 [21] D. Lovelock, *J. Math. Phys.* **13**, 874 (1972).
 [22] T. P. Sotiriou, *Lect. Notes Phys.* **892**, 3 (2015), arXiv:1404.2955 [gr-qc].
 [23] G. W. Horndeski, *Int. J. Theor. Phys.* **10**, 363 (1974).
 [24] L. Heisenberg, *JCAP* **05**, 015 (2014), arXiv:1402.7026 [hep-th].
 [25] P. Kanti, N. E. Mavromatos, J. Rizos, K. Tamvakis, and E. Winstanley, *Phys. Rev. D* **54**, 5049 (1996), arXiv:hep-th/9511071.
 [26] S. Alexander and N. Yunes, *Phys. Rept.* **480**, 1 (2009), arXiv:0907.2562 [hep-th].

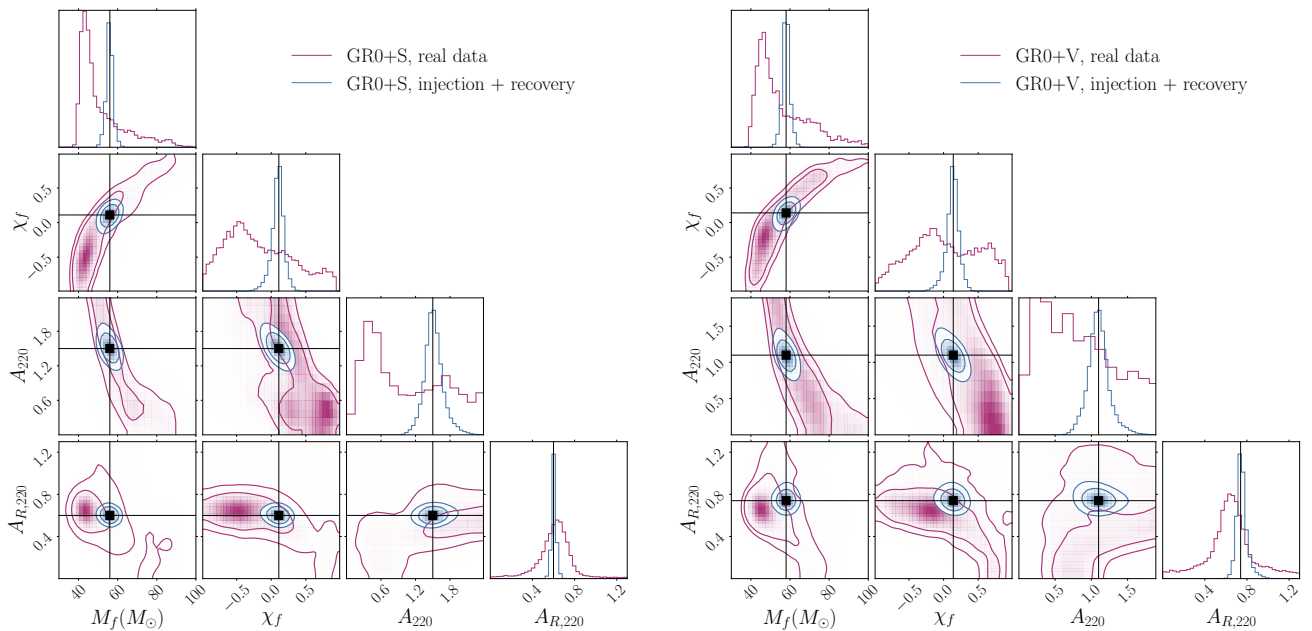


FIG. 6. Posterior distributions for real data (magenta) vs injection+recovery (blue) parameter estimation simulations with model GR0+S (left) and GR0+V (right). The levels of the 2D distributions indicate the 68% and the 90% credible intervals, while the black lines correspond to the injected values. Note that, in this case, we indicate the fundamental amplitude A_{220} rescaled by $d_L/M_f^{(m)}$, where $M_f^{(m)}$ is the final mass of the remnant expressed in meters.

- [27] S. Endlich, V. Gorbenko, J. Huang, and L. Senatore, *JHEP* **09**, 122 (2017), [arXiv:1704.01590 \[gr-qc\]](#).
- [28] T. Jacobson and D. Mattingly, *Phys. Rev. D* **64**, 024028 (2001), [arXiv:gr-qc/0007031](#).
- [29] P. Horava, *Phys. Rev. D* **79**, 084008 (2009), [arXiv:0901.3775 \[hep-th\]](#).
- [30] C. de Rham, G. Gabadadze, and A. J. Tolley, *Phys. Rev. Lett.* **106**, 231101 (2011), [arXiv:1011.1232 \[hep-th\]](#).
- [31] S. F. Hassan and R. A. Rosen, *JHEP* **02**, 126 (2012), [arXiv:1109.3515 \[hep-th\]](#).
- [32] C. Molina, P. Pani, V. Cardoso, and L. Gualtieri, *Phys. Rev. D* **81**, 124021 (2010), [arXiv:1004.4007 \[gr-qc\]](#).
- [33] P. Pani, *Int. J. Mod. Phys. A* **28**, 1340018 (2013), [arXiv:1305.6759 \[gr-qc\]](#).
- [34] V. Cardoso, W.-D. Guo, C. F. B. Macedo, and P. Pani, *Mon. Not. Roy. Astron. Soc.* **503**, 563 (2021), [arXiv:2009.07287 \[gr-qc\]](#).
- [35] S. Ma, L. Sun, and Y. Chen, *Phys. Rev. Lett.* **130**, 141401 (2023), [arXiv:2301.06705 \[gr-qc\]](#).
- [36] S. Ma, K. Mitman, L. Sun, N. Deppe, F. Hébert, L. E. Kidder, J. Moxon, W. Thrope, N. L. Vu, and Y. Chen, *Phys. Rev. D* **106**, 084036 (2022), [arXiv:2207.10870 \[gr-qc\]](#).
- [37] A. Maselli, P. Pani, L. Gualtieri, and E. Berti, *Phys. Rev. D* **101**, 024043 (2020), [arXiv:1910.12893 \[gr-qc\]](#).
- [38] G. Carullo, *Phys. Rev. D* **103**, 124043 (2021), [arXiv:2102.05939 \[gr-qc\]](#).
- [39] A. Maselli, S. Yi, L. Pierini, V. Vellucci, L. Reali, L. Gualtieri, and E. Berti, *Phys. Rev. D* **109**, 064060 (2024), [arXiv:2311.14803 \[gr-qc\]](#).
- [40] P. Pani and V. Cardoso, *Phys. Rev. D* **79**, 084031 (2009), [arXiv:0902.1569 \[gr-qc\]](#).
- [41] V. Cardoso and L. Gualtieri, *Phys. Rev. D* **80**, 064008 (2009), [Erratum: *Phys. Rev. D* **81**, 089903 (2010)], [arXiv:0907.5008 \[gr-qc\]](#).
- [42] P. Pani, E. Berti, and L. Gualtieri, *Phys. Rev. Lett.* **110**, 241103 (2013), [arXiv:1304.1160 \[gr-qc\]](#).
- [43] P. Pani, E. Berti, and L. Gualtieri, *Phys. Rev. D* **88**, 064048 (2013), [arXiv:1307.7315 \[gr-qc\]](#).
- [44] L. Pierini and L. Gualtieri, *Phys. Rev. D* **103**, 124017 (2021), [arXiv:2103.09870 \[gr-qc\]](#).
- [45] P. Wagle, N. Yunes, and H. O. Silva, *Phys. Rev. D* **105**, 124003 (2022), [arXiv:2103.09913 \[gr-qc\]](#).
- [46] P. A. Cano, K. Fransen, T. Hertog, and S. Maenaut, *Phys. Rev. D* **105**, 024064 (2022), [arXiv:2110.11378 \[gr-qc\]](#).
- [47] L. Pierini and L. Gualtieri, *Phys. Rev. D* **106**, 104009 (2022), [arXiv:2207.11267 \[gr-qc\]](#).
- [48] P. A. Cano, K. Fransen, T. Hertog, and S. Maenaut, *Phys. Rev. D* **108**, 124032 (2023), [arXiv:2307.07431 \[gr-qc\]](#).
- [49] P. Wagle, D. Li, Y. Chen, and N. Yunes, *Phys. Rev. D* **109**, 104029 (2024), [arXiv:2311.07706 \[gr-qc\]](#).
- [50] O. J. C. Dias, M. Godazgar, and J. E. Santos, *Phys. Rev. Lett.* **114**, 151101 (2015), [arXiv:1501.04625 \[gr-qc\]](#).
- [51] A. K.-W. Chung, P. Wagle, and N. Yunes, *Phys. Rev. D* **107**, 124032 (2023), [arXiv:2302.11624 \[gr-qc\]](#).
- [52] A. K.-W. Chung, P. Wagle, and N. Yunes, *Phys. Rev. D* **109**, 044072 (2024), [arXiv:2312.08435 \[gr-qc\]](#).
- [53] J. L. Blázquez-Salcedo, F. S. Khoo, J. Kunz, and L. M. González-Romero, *Phys. Rev. D* **109**, 064028 (2024), [arXiv:2312.10754 \[gr-qc\]](#).
- [54] A. K.-W. Chung and N. Yunes, (2024),

- arXiv:2405.12280 [gr-qc].
- [55] A. K.-W. Chung and N. Yunes, (2024), arXiv:2406.11986 [gr-qc].
- [56] J. L. Blázquez-Salcedo, C. F. B. Macedo, V. Cardoso, V. Ferrari, L. Gualtieri, F. S. Khoo, J. Kunz, and P. Pani, *Phys. Rev. D* **94**, 104024 (2016), arXiv:1609.01286 [gr-qc].
- [57] <https://pages.jh.edu/eberti2/ringdown/>.
- [58] <https://centra.tecnico.ulisboa.pt/network/grit/files/ringdown/>.
- [59] H. Takeda, A. Nishizawa, Y. Michimura, K. Nagano, K. Komori, M. Ando, and K. Hayama, *Phys. Rev. D* **98**, 022008 (2018), arXiv:1806.02182 [gr-qc].
- [60] H. Takeda, A. Nishizawa, K. Nagano, Y. Michimura, K. Komori, M. Ando, and K. Hayama, *Phys. Rev. D* **100**, 042001 (2019), arXiv:1904.09989 [gr-qc].
- [61] M. Isi and A. J. Weinstein, (2017), arXiv:1710.03794 [gr-qc].
- [62] R. Brito, A. Buonanno, and V. Raymond, *Phys. Rev. D* **98**, 084038 (2018), arXiv:1805.00293 [gr-qc].
- [63] G. Carullo, W. Del Pozzo, and J. Veitch, *Phys. Rev. D* **99**, 123029 (2019), [Erratum: *Phys. Rev. D* **100**, 089903 (2019)], arXiv:1902.07527 [gr-qc].
- [64] X. J. Forteza, S. Bhagwat, S. Kumar, and P. Pani, *Phys. Rev. Lett.* **130**, 021001 (2023), arXiv:2205.14910 [gr-qc].
- [65] V. Baibhav, M. H.-Y. Cheung, E. Berti, V. Cardoso, G. Carullo, R. Cotesta, W. Del Pozzo, and F. Duque, *Phys. Rev. D* **108**, 104020 (2023), arXiv:2302.03050 [gr-qc].
- [66] C. M. Biwer, C. D. Capano, S. De, M. Cabero, D. A. Brown, A. H. Nitz, and V. Raymond, *Publ. Astron. Soc. Pac.* **131**, 024503 (2019), arXiv:1807.10312 [astro-ph.IM].
- [67] B. P. Abbott *et al.* (LIGO Scientific, Virgo), *Phys. Rev. Lett.* **116**, 061102 (2016), arXiv:1602.03837 [gr-qc].
- [68] M. Giesler, M. Isi, M. A. Scheel, and S. Teukolsky, *Phys. Rev. X* **9**, 041060 (2019), arXiv:1903.08284 [gr-qc].
- [69] I. Ota and C. Chirenti, *Phys. Rev. D* **101**, 104005 (2020), arXiv:1911.00440 [gr-qc].
- [70] S. Bhagwat, X. J. Forteza, P. Pani, and V. Ferrari, *Phys. Rev. D* **101**, 044033 (2020), arXiv:1910.08708 [gr-qc].
- [71] J. Calderón Bustillo, P. D. Lasky, and E. Thrane, *Phys. Rev. D* **103**, 024041 (2021), arXiv:2010.01857 [gr-qc].
- [72] R. Cotesta, G. Carullo, E. Berti, and V. Cardoso, *Phys. Rev. Lett.* **129**, 111102 (2022), arXiv:2201.00822 [gr-qc].
- [73] M. Isi and W. M. Farr, (2022), arXiv:2202.02941 [gr-qc].
- [74] E. Finch and C. J. Moore, *Phys. Rev. D* **106**, 043005 (2022), arXiv:2205.07809 [gr-qc].
- [75] G. Carullo, R. Cotesta, E. Berti, and V. Cardoso, *Phys. Rev. Lett.* **131**, 169002 (2023), arXiv:2310.20625 [gr-qc].
- [76] S. Ma, L. Sun, and Y. Chen, *Phys. Rev. D* **107**, 084010 (2023), arXiv:2301.06639 [gr-qc].
- [77] R. Abbott *et al.* (LIGO Scientific, Virgo), *Phys. Rev. Lett.* **125**, 101102 (2020), arXiv:2009.01075 [gr-qc].
- [78] C. D. Capano, M. Cabero, J. Westerweck, J. Abedi, S. Kastha, A. H. Nitz, Y.-F. Wang, A. B. Nielsen, and B. Krishnan, *Phys. Rev. Lett.* **131**, 221402 (2023), arXiv:2105.05238 [gr-qc].
- [79] H. Siegel, M. Isi, and W. M. Farr, *Phys. Rev. D* **108**, 064008 (2023), arXiv:2307.11975 [gr-qc].
- [80] E. Maggio, H. O. Silva, A. Buonanno, and A. Ghosh, *Phys. Rev. D* **108**, 024043 (2023), arXiv:2212.09655 [gr-qc].
- [81] A. Gupta *et al.*, (2024), arXiv:2405.02197 [gr-qc].
- [82] A. H. Nitz, S. Kumar, Y.-F. Wang, S. Kastha, S. Wu, M. Schäfer, R. Dhurkunde, and C. D. Capano, (2021), arXiv:2112.06878 [astro-ph.HE].
- [83] S. A. Usman *et al.*, *Class. Quant. Grav.* **33**, 215004 (2016), arXiv:1508.02357 [gr-qc].
- [84] B. Zackay, T. Venumadhav, J. Roulet, L. Dai, and M. Zaldarriaga, *Phys. Rev. D* **104**, 063034 (2021), arXiv:1908.05644 [astro-ph.IM].
- [85] X. Jiménez Forteza, S. Bhagwat, P. Pani, and V. Ferrari, *Phys. Rev. D* **102**, 044053 (2020), arXiv:2005.03260 [gr-qc].
- [86] H. Jeffreys, *The Theory of Probability*, Oxford Classic Texts in the Physical Sciences (1939).
- [87] S. Bhagwat, C. Pacilio, E. Barausse, and P. Pani, *Phys. Rev. D* **105**, 124063 (2022), arXiv:2201.00023 [gr-qc].
- [88] S. Bhagwat, C. Pacilio, P. Pani, and M. Mapelli, *Phys. Rev. D* **108**, 043019 (2023), arXiv:2304.02283 [gr-qc].
- [89] V. Kalogera *et al.*, (2021), arXiv:2111.06990 [gr-qc].
- [90] D. Reitze *et al.*, *Bull. Am. Astron. Soc.* **51**, 035 (2019), arXiv:1907.04833 [astro-ph.IM].
- [91] M. Evans *et al.*, (2021), arXiv:2109.09882 [astro-ph.IM].
- [92] M. Evans *et al.*, (2023), arXiv:2306.13745 [astro-ph.IM].
- [93] S. Hild *et al.*, *Class. Quant. Grav.* **28**, 094013 (2011), arXiv:1012.0908 [gr-qc].
- [94] M. Maggiore *et al.*, *JCAP* **03**, 050 (2020), arXiv:1912.02622 [astro-ph.CO].
- [95] M. Branchesi *et al.*, *JCAP* **07**, 068 (2023), arXiv:2303.15923 [gr-qc].
- [96] M. Colpi *et al.*, (2024), arXiv:2402.07571 [astro-ph.CO].
- [97] E. Berti, A. Sesana, E. Barausse, V. Cardoso, and K. Belczynski, *Phys. Rev. Lett.* **117**, 101102 (2016), arXiv:1605.09286 [gr-qc].
- [98] M. Okounkova, L. C. Stein, J. Moxon, M. A. Scheel, and S. A. Teukolsky, *Phys. Rev. D* **101**, 104016 (2020), arXiv:1911.02588 [gr-qc].
- [99] M. Okounkova, *Phys. Rev. D* **102**, 084046 (2020), arXiv:2001.03571 [gr-qc].
- [100] W. E. East and J. L. Ripley, *Phys. Rev. D* **103**, 044040 (2021), arXiv:2011.03547 [gr-qc].
- [101] W. E. East and J. L. Ripley, *Phys. Rev. Lett.* **127**, 101102 (2021), arXiv:2105.08571 [gr-qc].
- [102] P. Figueras and T. França, *Phys. Rev. D* **105**, 124004 (2022), arXiv:2112.15529 [gr-qc].
- [103] L. Aresté Saló, K. Clough, and P. Figueras, *Phys. Rev. Lett.* **129**, 261104 (2022), arXiv:2208.14470 [gr-qc].
- [104] M. Corman, J. L. Ripley, and W. E. East, *Phys. Rev. D* **107**, 024014 (2023), arXiv:2210.09235 [gr-qc].
- [105] R. Cayuso, P. Figueras, T. França, and L. Lehner, *Phys. Rev. Lett.* **131**, 111403 (2023), arXiv:2303.07246 [gr-qc].
- [106] N. Yunes and F. Pretorius, *Phys. Rev. D* **79**, 084043 (2009), arXiv:0902.4669 [gr-qc].